MoO_2/Mo_2C Heteronanotubes Function as High-Performance Li-Ion Battery Electrode

Hao-Jie Zhang, Kai-Xue Wang, Xue-Yan Wu, Yan-Mei Jiang, Yu-Bo Zhai, Cheng Wang, Xiao Wei, and Jie-Sheng Chen**

Instead of carbon, Mo_2C is used to modify the MoO_2 material for the first time. The presence of highly conductive and electrochemical inactive Mo_2C decreases the resistance of the charge transport and enhances the structural stability of MoO_2 nanoparticles upon lithiation and delithiation, ensuring the superior cycling stability and high rate capability of the heteronanotubes. Cycled at 200 and 1000 mA g^{-1} for 140 cycles, the discharge capacities of the MoO_2/Mo_2C heteronanotubes remain to be 790 and 510 mAh g^{-1}, respectively. This work demonstrates the potential of the novel heteronanotubes for application as an electrode material for high-performance Li-ion batteries.

1. Introduction

Lithium ion batteries (LIBs) have been successfully adopted as energy sources for a wide range of portable electronic devices. With the merits of high energy density, long cycle life and low cost, LIBs are also considered as the promising energy storage devices for electric vehicles (EVs) and hybrid electric vehicles (HEVs).[1] In the past decades, metal oxides with high theoretical capacities have gained a great deal of attention in LIBs field.[2] Among these metal oxides, molybdenum dioxide (MoO_2) is one of the most attractive host materials for the storage of lithium ions. Molybdenum dioxide possesses many attractive properties, such as rich chemistry associated with multiple valence states, high electrochemical activity toward lithium, and low electrical resistivity.[3] However, MoO_2 suffers from serious capacity fading caused by large volume change and sluggish kinetics during the charge/discharge processes.

Formation of a hierarchical porous structure and carbon coating are generally used to improve the electrochemical performances of MoO_2. Hierarchical porous structures, such as microcapsules[4] and net[2f] can accommodate the volume variation of the electrode material upon cycling, improving the structural stability and thus the cycleability. However, the rate capability of these hierarchical porous structures is still unsatisfactory due to the sluggish kinetics of MoO_2. Surface modification with highly conductive carbon is a common strategy to enhance the electrochemical performance of electrode materials. Carbon-coated MoO_2 nanobelts[5] and nanowires[6] delivered higher charge/discharge capacities than unadulterated MoO_2. However, the carbon content in these carbon/MoO_2 composites is hard to control. Due to the high content of the electrochemical active carbon, the specific capacities of the composite materials are usually much lower than the theoretical capacity of MoO_2 and no distinct charge/discharge plateaus of MoO_2 are observed, as for hard carbon materials. Thus, new approaches are highly desired to enhance the electrochemical performance of MoO_2 to a greater extent.

Recently, heteronanostructures have attracted a lot of attention due to the specific synergy between different nanoparticles.[7] A variety of materials with a heteronanostructure have been prepared in the past but the preparation approaches are usually sophisticated. Herein, a simple one-step carbothermal reduction method is developed for the preparation of hierarchical porous MoO_2/Mo_2C heteronanotubes by using a mesoporous carbon CMK-3 as both the template and the reactant. Instead of carbon, we use Mo_2C to modify the MoO_2 material for the first time. The electrochemical inactive Mo_2C with a high specific conductance of 1.02×10^2 S cm^{-1} distinctly increases the structural stability and electronic conductivity of the heteronanotubes.[8] Taking advantage of the combination of an appropriate amount of Mo_2C and the hierarchical porous structure, the cycling and rate performance of the heteronanotubes is markedly enhanced. At a current density of 1000 mA g^{-1}, a discharge capacity of approximately 510 mAh g^{-1} is still retained over 140 cycles.

H.-J. Zhang, Prof. K.-X. Wang, Y.-M. Jiang, Y.-B. Zhai, C. Wang, Dr. W. Xiao, Prof. J.-S. Chen
School of Chemistry and Chemical Engineering
Shanghai Jiao Tong University
Shanghai, 200240, China
E-mail: k.wang@sjtu.edu.cn; chemcj@sjtu.edu.cn
Dr. X.-Y. Wu
School of Materials Science and Engineering
Shanghai Jiao Tong University
Shanghai, 200240, China

DOI: 10.1002/adfm.201303856

2. Results and Discussion

2.1. Formation of the MoO_2/Mo_2C Heteronanotubes

The hierarchical porous MoO_2/Mo_2C heteronanotubes were fabricated by using MoO_3 as a Mo source and mesoporous carbon CMK-3 as a template and reactant via a route illustrated in **Scheme 1**. First, CMK-3 was prepared following a procedure reported in the literature.[9] The morphology and

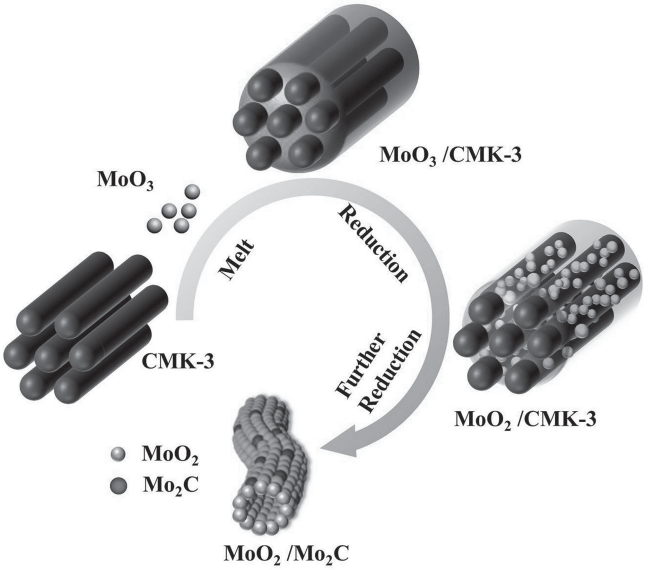

Scheme 1. The schematic illustration of the preparation of MoO_2/Mo_2C heteronanotubes.

the mesoporous feature of CMK-3 were characterized by low-angle X-ray diffraction (XRD), scanning electron microscopy (SEM) and transmission electron microscopy (TEM) analyses (Figures S1,S2, Supporting Information). Second, the reactants MoO_3 and CMK-3 were mixed together and ground for 20 min. Then, the mixture was heated to 820 °C, over the melting point of MoO_3 (795 °C). The molten MoO_3 was dispersed onto the surface of CMK-3 and gradually reduced to MoO_2 by CMK-3 (Equation 1). MoO_2 nanoparticles with a higher melting point were deposited over the outer surface of CMK-3 rods. Further reaction of MoO_2 nanoparticles with CMK-3 led to the formation of Mo_2C nanoparticles, generating the MoO_2/Mo_2C heterostructure (Equation 2). The consumption of CMK-3 upon the reaction with Mo species left a nano-sized tubular structure behind. The nanotubes together with the voids among the MoO_2 and Mo_2C nanoparticles generate a hierarchical porous structure.

$$MoO_3 + C \rightarrow MoO_2 + CO_x \quad (1)$$

$$MoO_2 + C \rightarrow Mo_2C + CO_x \quad (2)$$

2.2. Characterizations of the MoO_2/Mo_2C Heteronanotubes

The XRD pattern of the hierarchical porous MoO_2/Mo_2C heteronanotubes is shown in **Figure 1**a. The pattern fits well with the monoclinic MoO_2 with a space group of $P2_1/c$ (JCPDS 65–5758) and hexagonal α-Mo_2C with a space group of $P6_3/mmc$ (JCPDS 35–787). The sharp peaks with a high intensity indicate the high crystallinity of the heterostrctured material. The well resolved diffraction peaks located at 26.0°, 37.2°, and 53.6° are ascribed to the (011), (200), and (220) planes of MoO_2, while the diffraction peaks located at 34.5°, 38.0°, and 39.5° can be readily assigned to the (100), (002), and (101) planes of the hexagonal α-Mo_2C. No diffractions corresponding to MoO_3 are observed, indicating that all of the Mo species are transformed into MoO_2 and α-Mo_2C in the presence of carbon. It is believed that no

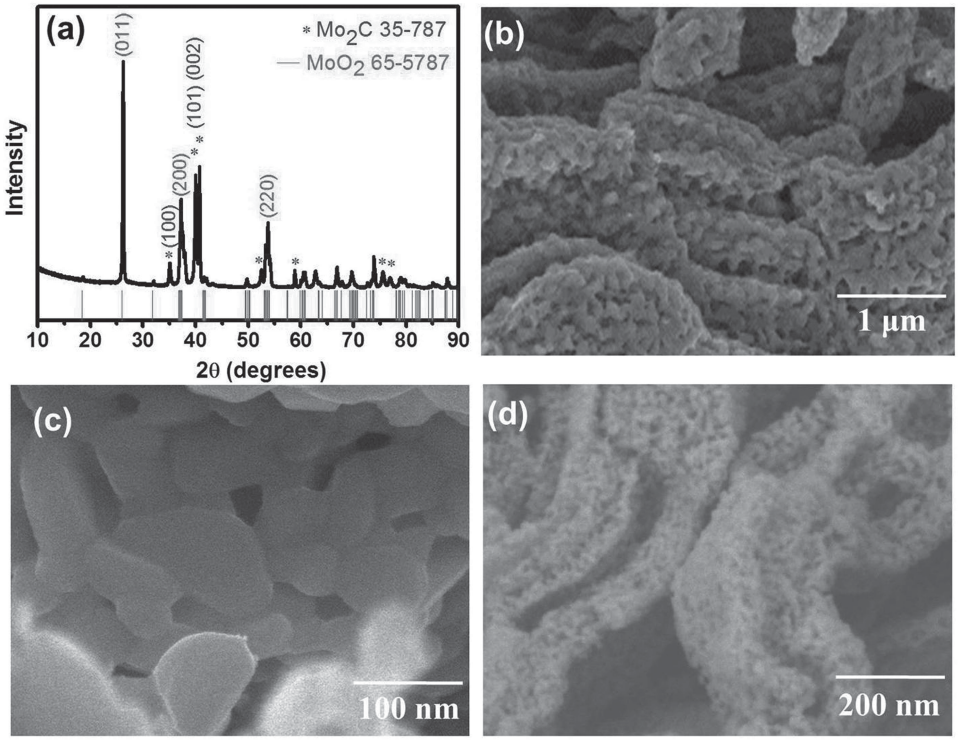

Figure 1. a) XRD pattern and b–d) SEM images of the MoO_2/Mo_2C heteronanotubes.

CMK-3 was left after the reduction reaction between MoO_2 and carbon because if any excessive carbon was left, MoO_2 would be completely converted to α-Mo_2C (Figure S3, Supporting Information). The content of α-Mo_2C in the heteronanotubes is determined to be approximately 30 wt% by dissolving the MoO_2 component in the heteronanotubes in hot HNO_3 aqueous solution. Thus, the weight ratio of MoO_2 to Mo_2C in the heteronanotube is 70:30.

Both SEM and TEM were used to reveal the morphological and textural details of the obtained hierarchical porous MoO_2/Mo_2C heteronanotubes. The morphology of the heteronanotubes (Figure 1b) closely mimics that of the CMK-3 as shown in Figure S1c (Supporting Information), indicating the templating effect of CMK-3 for the formation of the tubular morphology. The nanotubular structure generated through the consumption of the CMK-3 template can be observed from the open nanotubes in the SEM image (Figure 1d). The inner diameter of the nanotube is less than 100 nm and the length is about 1.0 μm. The nanotubes are built up by nanoparticles with a relatively smooth surface. The diameter of the nanoparticles ranges from 50 to 100 nm (Figure 1c). The aggregation of such nanoparticles leads to the formation of mesopores with a dimension of about 30 nm in diameter (Figure 1c). The combination of the mesopores with the nanotubes generates a hierarchical structure with a 3D porous network, facilitating the penetration of electrolyte and lithium ions within the electrode (**Figure 2**a). The high-resolution transmission electron microscopy (HRTEM) images of the sample are shown in Figure 2b. The lattice fringes of approximately 3.40 and 2.28 Å are ascribed to the (011) plane of MoO_2 and the (101) plane of Mo_2C, respectively. The HRTEM observation demonstrates that the hierarchical porous nanotubes are composed of both MoO_2 and Mo_2C nanoparticles. It is also observed in the SEM and HRTEM images that MoO_2 and Mo_2C nanoparticles are well bound together, increasing the stability of the hierarchical porous structure and at the same time decreasing the grain boundary resistance.

The nitrogen adsorption-desorption isotherms and the corresponding pore size distribution curve of the hierarchical porous MoO_2/Mo_2C heteronanotubes are shown in Figure S4 (Supporting Information). The isotherms at a relative pressure of 0.4–0.7 can be classified as type IV, typical of mesoporous material. The adsorption and desorption activity at a high relative pressure indicate the presence of macropores derived from the accumulation of MoO_2 and Mo_2C nanoparticles. This MoO_2/Mo_2C heteronanotubes has a total BET surface of 62.8 $m^2\ g^{-1}$ and a pore volume of 0.134 $cm^3\ g^{-1}$.

2.3. Electrochemical Performances of the MoO_2/Mo_2C Heteronanotubes

The cyclic voltammetry (CV) curve of the hierarchical porous MoO_2/Mo_2C heteronanotubes at 0.5 mV s^{-1} over a voltage range of 0.01 and 3.0 V is shown in **Figure 3**a. During the first cycle, two pronounced reduction peaks located at 1.13 and 1.40 V are observed. In the subsequent cycles, these two peaks shift to 1.27 and 1.52 V. The shift is attributed to the phase transformations between the monoclinic and orthorhombic phases in the partially lithiated Li_xMoO_2.[10] These two phase transformations are highly reversible in the subsequent cycles as indicated by the two pronounced reduction/oxidation pairs even after 10 cycles. Neither reduction nor oxidation peaks of Mo_2C can

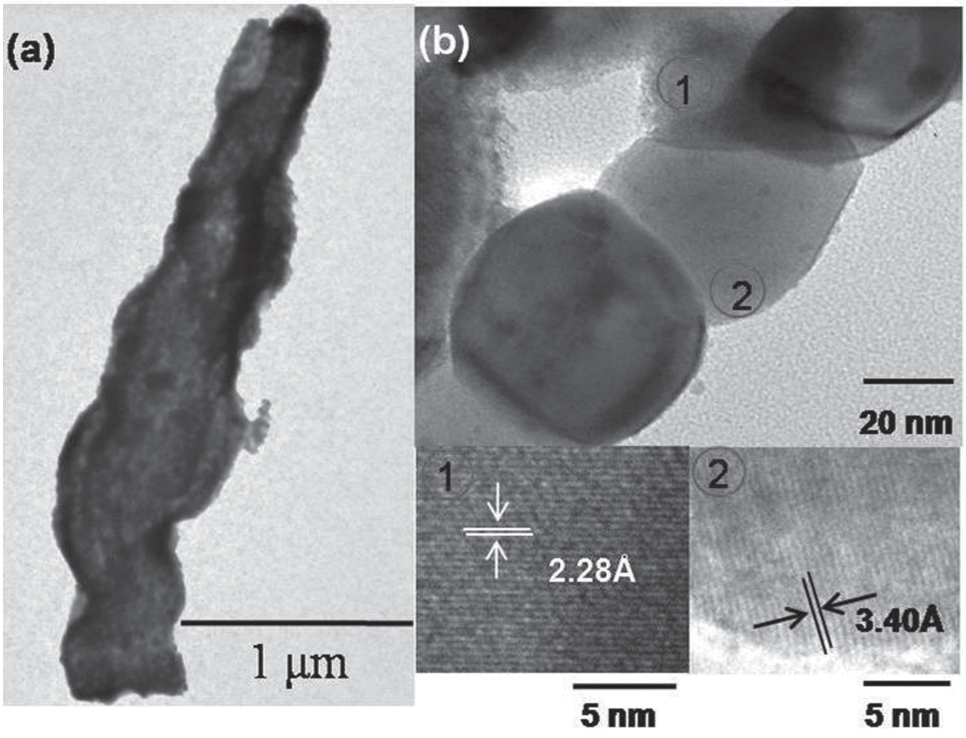

Figure 2. a) TEM and b) HRTEM images of the MoO_2/Mo_2C heteronanotubes.

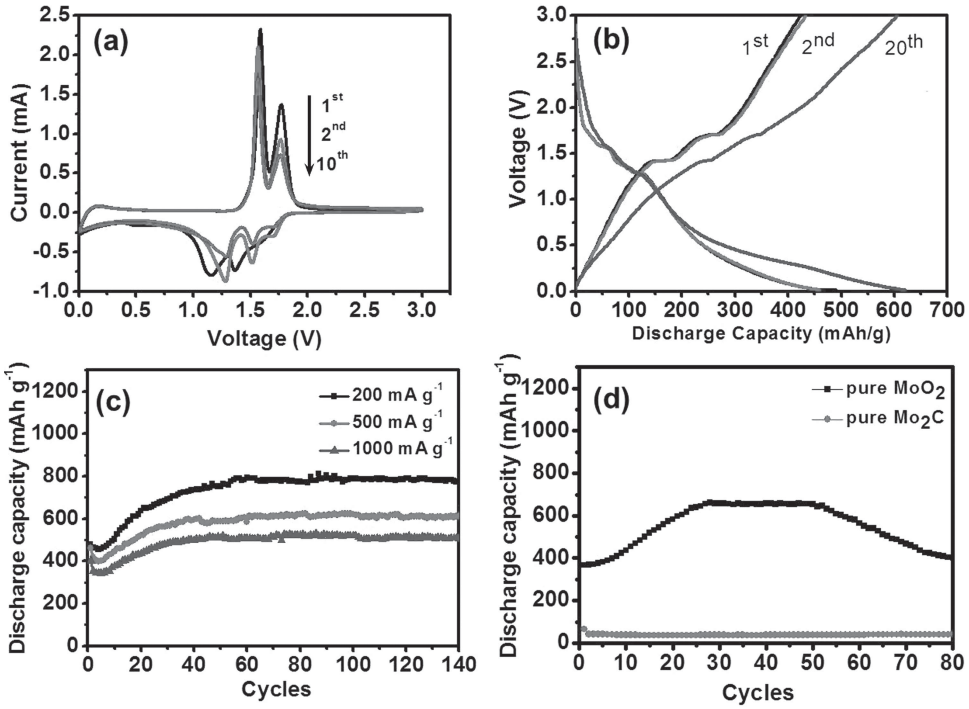

Figure 3. a) Cyclic voltammogram of MoO_2/Mo_2C heteronanotubes at a scan rate of 0.5 mV s^{-1}; b) galvanostatic charge/discharge curves of MoO_2/Mo_2C heteronanotubes at a current density of 200 mA g^{-1}; c) cycling performance of MoO_2/Mo_2C heteronanotubes at different current densities, and d) cycling performances of pure hierarchical MoO_2 and pure Mo_2C at a current density of 200 mA g^{-1}.

be observed since Mo_2C has no electrochemical activities over the voltage range of 0.01–3.0 V (Figure S5, Supporting Information). The intensities of these two reduction/oxidation peak pairs gradually decrease in the subsequent cycles, typical for MoO_2 materials. The charge and discharge processes of MoO_2 can be divided into two parts over a voltage range of 0.01–3.0 V. Over 1.0 V, lithium ions are inserted into the structure of MoO_2, resulting in the formation of Li_xMoO_2. When discharged to potentials lower than 1.0 V, Li_xMoO_2 would gradually convert to Mo metal and Li_2O, leading to the decrease in intensity of the intercalation and deintercalation peaks with cycles.

The charge/discharge curves of the hierarchical porous MoO_2/Mo_2C heteronanotubes at a current density of 200 mA g^{-1} over a voltage range of 0.01–3.0 V are shown in Figure 3b. The initial discharge and charge capacities of the MoO_2/Mo_2C heteronanotubes calculated based on the total weight of the composite are approximately 480 and 410 mAh g^{-1}, respectively, giving a Coulombic efficiency of 85.8%. The capacities are mainly attributed to MoO_2 in the heteronanotubes because the electrochemical inactive Mo_2C gives no contribution to the specific capacities. The capacity loss (14.2%) of the initial cycle is attributed to the irreversible processes, such as the trapping of some lithium in the lattice of MoO_2, the formation of solid electrolyte interface (SEI), and the decomposition of the electrolyte molecules. Two pronounced charge plateaus at 1.4 and 1.7 V are observed and they remain even after 20 cycles (Figure 3b). Such distinct plateaus have seldom been detected for MoO_2/C composite materials reported in the literature.[6,11] The lithium ion insertion and extraction behaviors for MoO_2/C composite materials are usually similar to that of hard carbon materials due to the high content of carbon. For the MoO_2/Mo_2C heteronanotubes, the presence of distinct plateaus indicates that the introduction of Mo_2C gives negligible influence on the lithium ion insertion and extraction behaviors of MoO_2. Meanwhile, the hierarchical porous structure effectively buffers the volume change and maintains the charge and discharge plateaus during the charge and discharge process. After 20 cycles, the discharge capacity increases to 630 mAh g^{-1} and the charge capacity to 610 mAh g^{-1}. The increase of the charge and discharge capacities and the decrease of the plateau length are attributed to the gradual transformation of Li_xMoO_2 to Mo upon cycling.

The cycling performances of the hierarchical porous MoO_2/Mo_2C heteronanotubes at different current densities are shown in Figure 3c. The heteronanotubes exhibit a high discharge/charge capacity and super cycling performance at the current density of 200 mA g^{-1}. Within the initial 50 cycles, the discharge capacity of the heteronanotubes gradually increases from 480 to 790 mAh g^{-1}. This increase is attributed to the activation of the electrode material, in good agreement with the CV results and those reported in the literature.[2b,2f,12] After 50 cycles, such high discharge capacity is well maintained. The heteronanotubes also show good Coulombic efficiency. When cycled at 200 mA g^{-1}, the Coulombic efficiency of the first cycle is 85.8% and increases to 91.4% in the second cycle. The Coulombic efficiency of over 97.8% is well maintained in the following cycles (Figure S6, Supporting Information). The high Coulombic efficiency is attributed to the stable hierarchical porous heterostructure.

The hierarchical porous MoO_2/Mo_2C heteronanotubes also exhibit excellent rate capability. When cycled at 500 and

1000 mA g^{-1}, similar increase in discharge capacity can be observed within the initial 30 cycles. But the activation process of the electrode is obviously shortened through the increase in current density. Cycled at 500 and 1000 mA g^{-1} for 140 cycles, the discharge capacities reach 623 and 510 mAh g^{-1}, respectively. The cycling stability and rate capability of the heteronanotubes are obviously superior over those of MoO_2 materials reported in the literature which are usually suffered from dramatic capacity fading after several ten cycles.[6,13] For example, MoO_2 with different hierarchical porous structures have been prepared.[2f,12] However, few such hierarchical porous MoO_2 materials can maintain the high charge and discharge capacities for 100 cycles. For comparison, MoO_2 material with an identical hierarchical porous structure has also been prepared through the carbothermal reduction method by using CMK-3 (0.1 g) and MoO_3 (1.0 g) as reactants (Figure S7, Supporting Information). The cycling performance of the hierarchical porous MoO_2 at 200 mA g^{-1} is shown in Figure 3d. An increase in discharge capacity is observed and the capacity reaches 650 mAh g^{-1} after 50 cycles. The activation process for the hierarchical porous MoO_2 is similar to that of the MoO_2/Mo_2C heteronanotubes. However, the discharge capacity of the hierarchical porous MoO_2 decreases dramatically after the activation process. A capacity of only 400 mAh g^{-1} is retained after 80 cycles. Given the fact that the pure MoO_2 and MoO_2/Mo_2C heteronanotubes have an identical hierarchical porous structure, the super cycling performance of the MoO_2/Mo_2C heteronanotubes is mainly attributed to the presence of highly conductive Mo_2C nanoparticles. The Mo_2C nanoparticles attached tightly with MoO_2 nanoparticles significantly increase the electronic conductivity of the heteronanotubes and reduce the grain boundary resistance, resulting in the high rate capability (Table S1, Supporting Information). In addition, Mo_2C is also expected to function as a support to maintain the structural stability of the heteronanotubes upon cycling. MoO_2/Mo_2C heteronanotubes can be prepared through the reaction of MoO_3 and CMK-3 with weight ratios of MoO_3 to CMK-3 ranging from 4:1 to 7:1. The electrochemical performances of these heterostructures are evaluated by galvanostatic charge-discharge tests at a current density of 200 mA g^{-1} (Figure S8, Supporting Information). The heteronanotubes that have a MoO_2 to Mo_2C weight ratio of 70:30 prepared with MoO_3 to CMK-3 ratio of 5:1 exhibits the best cycling performances and rate capability.

Therefore, the high electrochemical performances are ascribed to the unique structural feature of the MoO_2/Mo_2C heteronanotubes and the presence of Mo_2C (Schematically illustrated in **Figure 4**). The size of MoO_2 nanoparticles within the heteronanotubes is around 50 nm, significantly shortening the diffusion length of lithium ions. The Mo_2C nanoparticles with a high electronic conductivity significantly decrease the resistance of the heteronanotubes electrode. The electrochemical inactive Mo_2C nanoparticles also increase the structural stability of the heteronanotubes. The hierarchical porous structure generated by the 1D nanotubes and the void spaces among the nanoparticles within the wall of the nanotubes provides a 3D transport pathway for the electrolyte and lithium ions, enhancing the rate capability of the MoO_2/Mo_2C material. It is also envisaged that the large volume variation during the cycling can be well accommodated by hierarchical porous structure, ensuring the high cycling stability. In addition, the good

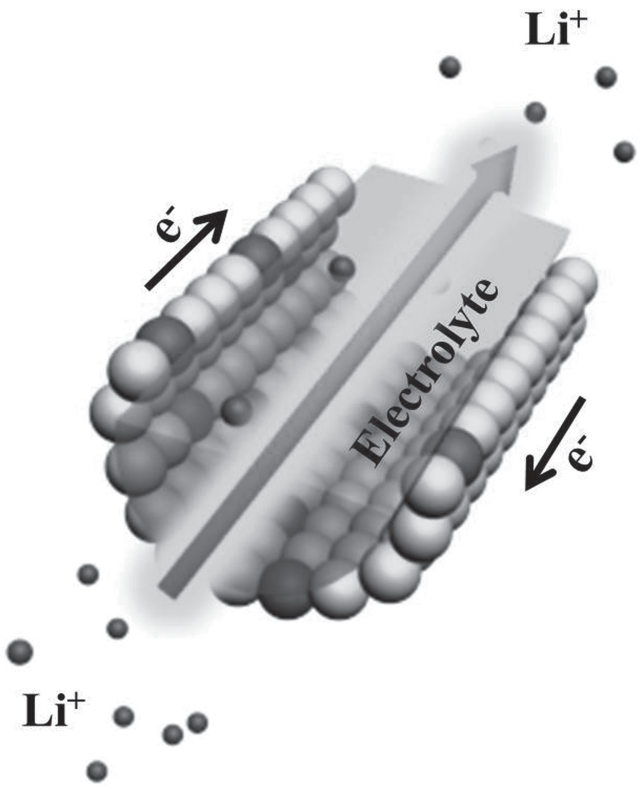

Figure 4. The schematic representation of the transport pathways of lithium ions and electrons in hierarchical porous MoO_2/Mo_2C heteronanotubes.

contact among MoO_2 and Mo_2C nanoparticles as revealed by the HRTEM observation reduces the resistance of the interparticle boundary interfaces, benefiting the rate performance.

3. Conclusion

In summary, we have successfully prepared hierarchical porous MoO_2/Mo_2C heteronanotubes through a one-step carbothermal reduction method. The nanotubular structure of the sample is attributed to the consumption of the CMK-3 template. The nanotubes are built up by nanoparticles with a relatively smooth surface. Cycled at 500 and 1000 mA g^{-1} for 140 cycles, the discharge capacities reach 623 and 510 mAh g^{-1}, respectively. The high electrochemical performance of the heteronanotubes is attributed to their unique hierarchical porous structure and the presence of Mo_2C species. The hierarchical porous structure facilitates the transportation of the electrolyte and lithium ions and enhances the structural stability of the heteronanotubes through the accommodation of volume variation upon cycling. The electrochemical inactive Mo_2C increases the electronic conductivity and stability of the heteronanotubes, contributing to the high rate capability and long cycling stability. The MoO_2/Mo_2C heteronanotubes are a promising anode material for high performance LIBs. Meanwhile, the carbothermal reduction approach developed in this work may also be applicable to the preparation of other metal oxides with hierarchical porous structures.

4. Experimental Section

Preparation of Materials: P123 ($EO_{20}PPO_{70}EO_{20}$, 2.0 g) was dissolved in HCl aqueous solution (2.0 M, 60 mL) at 38 °C. Tetraethylorthosilicate (4.2 g) was added to the above solution with vigorous stirring. The solution was stirred for 6 min and kept still for 24 h at 38 °C. Then, the precursor was loaded into an autoclave and heated at 100 °C for 24 h. The product was collected by filtration, dried and calcined at 550 °C in air to remove the surfactant. Sucrose (1.25 g) was dissolved in water (5.0 mL) containing H_2SO_4 (0.14 g). Surfactant-free SBA-15 (1.0 g) was then dispersed in the above solution. After sonicated for 1 h, the mixture was heated at 100 °C for 12 h and at 160 °C for another 12 h. The impregnation process was repeated once with another aqueous solution (5.0 mL) containing sucrose (0.8 g) and H_2SO_4 (0.09). The composite was completely carbonized at 900 °C for 5 h in an argon atmosphere. CMK-3 was obtained through the removal of SBA-15 in a 5% HF aqueous solution at room temperature.

MoO_2/Mo_2C heteronanotubes was prepared through a carbothermal reduction route. MoO_3 (0.5 g) and CMK-3 (0.1 g) were mixed and ground for 20 min. Then the mixture was subsequently treated at 820 °C in a N_2 atmosphere for 90 min. Finally, the black-colored product was collected for further characterization. For comparison, samples were also prepared by ranging the MoO_3 to CMK-3 weight ratios under the same conditions. Mo_2C was bought from Hunan Guangyuan company without further treatment.

Characterization: The X-ray diffraction (XRD) pattern of the as-prepared product was characterized by Rigaku D/max-2200/PC X-Ray diffractometer at a scanning rate of 2° min^{-1}. The morphology and crystal lattice of the sample were elucidated on the basis of transmission electron microscopy (TEM) on a JEOL JEM-100CX microscope with an accelerating voltage of 100 kV, high-resolution TEM on a JEOL JEM-2100F microscope with an accelerating voltage of 200 kV, and field-emission scanning electron microscopy (FE-SEM) on a JEOL JSM-6700F microscope with an accelerating voltage of 5 kV. The brunauer-emmett-teller (BET) surface area and porosity were determined by nitrogen adsorption-desorption using a Nova 2200e surface area/pore size analyzer.

Electrochemical Measurements: The MoO_2/Mo_2C heteronanotubes, acetylene black, and poly (vinylidene fluoride) (PVDF) binder were mixed at a weight ratio of 80:10:10 and dispersed in a N-methylpyrrolidone (NMP) solution to form a slurry. The slurry was coated on copper foil and dried in a vacuum oven at 110 °C overnight prior to coin-cell assembly. The cells (CR2016 type coin cells) were assembled in a glove box filled with ultra-high purity argon using polypropylene membrane (UBE Industries Ltd.) as the separator, Li metal as the anode, and 1 M $LiPF_6$ in ethyl carbonate/dimethyl carbonate (EC/DEC) (1:1 v/v) as the electrolyte. The charge and discharge performance of the electrodes was evaluated at room temperature using a Land CT2001A battery test system. The cyclic voltammetry (CV) curves were obtained on a Chenhua CHI 660B electrochemical station. For comparison, the electrochemical performances of pure MoO_2 and Mo_2C were elevated under the same conditions.

Supporting Information

Supporting Information is available from the Wiley Online Library or from the author.

Acknowledgements

This work was financially supported by the National Basic Research Program of China (2013CB934102, 2011CB808703) and the National Natural Science Foundation of China.

Received: November 14, 2013
Revised: December 21, 2013
Published online: February 12, 2014

[1] a) J. M. Tarascon, M. Armand, *Nature* **2001**, *414*, 359; b) B. Dunn, H. Kamath, J. M. Tarascon, *Science* **2011**, *334*, 928; c) M. S. Whittingham, *Chem. Rev.* **2004**, *104*, 4271.
[2] a) J. Chen, L. Xu, W. Li, X. Gou, *Adv. Mater.* **2005**, *17*, 582; b) Y. Shi, B. Guo, S. A. Corr, Q. Shi, Y. S. Hu, K. R. Heier, L. Chen, R. Seshadri, G. D. Stucky, *Nano Lett.* **2009**, *9*, 4215; c) F. Jiao, P. G. Bruce, *Adv. Mater.* **2007**, *19*, 657; d) W. Y. Li, L. N. Xu, J. Chen, *Adv. Funct. Mater.* **2005**, *15*, 851; e) B. Guo, X. Fang, B. Li, Y. Shi, C. Ouyang, Y. S. Hu, Z. Wang, G. D. Stucky, L. Chen, *Chem. Mater.* **2011**, *24*, 457; f) Y. Sun, X. Hu, J. C. Yu, Q. Li, W. Luo, L. Yuan, W. Zhang, Y. Huang, *Energy Environ. Sci.* **2011**, *4*, 2870.
[3] a) S. H. Lee, Y. H. Kim, R. Deshpande, P. A. Parilla, E. Whitney, D. T. Gillaspie, K. M. Jones, A. H. Mahan, S. Zhang, A. C. Dillon, *Adv. Mater.* **2008**, *20*, 3627; b) L. Q. Mai, B. Hu, W. Chen, Y. Y. Qi, C. S. Lao, R. S. Yang, Y. Dai, Z. L. Wang, *Adv. Mater.* **2007**, *19*, 3712; c) L. Zhou, H. B. Wu, Z. Wang, X. W. Lou, *ACS Appl. Mater. Interfaces* **2011**, *3*, 4853.
[4] X. Zhao, M. Cao, B. Liu, Y. Tian, C. Hu, *J. Mater. Chem.* **2012**, *22*, 13334.
[5] L. Yang, L. Liu, Y. Zhu, X. Wang, Y. Wu, *J. Mater. Chem.* **2012**, *22*, 13148.
[6] Q. Gao, L. Yang, X. Lu, J. Mao, Y. Zhang, Y. Wu, Y. Tang, *J. Mater. Chem.* **2010**, *20*, 2807.
[7] a) Z. Peng, H. Yang, *J. Am. Chem. Soc.* **2009**, *131*, 7542; b) S. Zhou, X. Liu, D. Wang, *Nano Lett.* **2010**, *10*, 860; c) Y. Kim, J. W. Hong, Y. W. Lee, M. Kim, D. Kim, W. S. Yun, S. W. Han, *Angew. Chem.* **2010**, *122*, 10395; *Angew. Chem. Int. Ed.* **2010**, *49*, 10197; d) S. Shen, Y. Zhang, L. Peng, Y. Du, Q. Wang, *Angew. Chem.* **2011**, *123*, 7253; *Angew. Chem. Int. Ed.* **2011**, *50*, 7115; e) L. Ji, Z. Lin, M. Alcoutlabi, X. Zhang, *Energy Environ. Sci.* **2011**, *4*, 2682; f) L. Ji, Z. Lin, B. Guo, A. J. Medford, X. Zhang, *Chem. Eur. J.* **2010**, *16*, 11543; g) L. Ji, A. J. Medford, X. Zhang, *J. Mater. Chem.* **2009**, *19*, 5593; h) L. Ji, Z. Tan, T. Kuykendall, E. J. An, Y. Fu, V. Battaglia, Y. Zhang, *Energy Environ. Sci.* **2011**, *4*, 3611; i) L. Ji, Z. Tan, T. R. Kuykendall, S. Aloni, S. Xun, E. Lin, V. Battaglia, Y. Zhang, *Phys. Chem. Chem. Phys.* **2011**, *13*, 7170; j) L. Ji, O. Toprakci, M. Alcoutlabi, Y. Yao, Y. Li, S. Zhang, B. Guo, Z. Lin, X. Zhang, *ACS Appl. Mater. Interfaces* **2012**, *4*, 2672; k) Z. Lin, L. Ji, M. D. Woodroof, X. Zhang, *J. Power Sources* **2010**, *195*, 5025.
[8] H. O. Pierson, Handbook of Refractory Carbides and Nitrides, Noyes Publications, New Jersey **1996**.
[9] X. Ji, K. T. Lee, L. F. Nazar, *Nat. Mater.* **2009**, *8*, 500.
[10] J. R. Dahn, W. R. McKinnon, *Solid State Ionics* **1987**, *23*, 1.
[11] a) Y. Sun, X. Hu, W. Luo, Y. Huang, *J. Mater. Chem.* **2012**, *22*, 425; b) Z. Wang, J. S. Chen, T. Zhu, S. Madhavi, X. W. Lou, *Chem. Commun.* **2010**, *46*, 6906.
[12] Y. Sun, X. Hu, W. Luo, Y. Huang, *ACS Nano* **2011**, *5*, 7100.
[13] X. Ji, P. S. Herle, Y. Rho, L. F. Nazar, *Chem. Mater.* **2007**, *19*, 374.